



12-2006

# Spatial Grain Size Sorting in Eolian Ripples and Estimation of Wind Conditions on Planetary Surfaces: Application to Meridiani Planum, Mars

Douglas J. Jerolmack  
*University of Pennsylvania*, [sediment@sas.upenn.edu](mailto:sediment@sas.upenn.edu)


David Mohrig

John P. Grotzinger

David A. Fike

Wesley A. Watters

Follow this and additional works at: [http://repository.upenn.edu/ees\\_papers](http://repository.upenn.edu/ees_papers)

 Part of the [Environmental Sciences Commons](#), [Physical Processes Commons](#), and the [Sedimentology Commons](#)

## Recommended Citation

Jerolmack, D. J., Mohrig, D., Grotzinger, J. P., Fike, D. A., & Watters, W. A. (2006). Spatial Grain Size Sorting in Eolian Ripples and Estimation of Wind Conditions on Planetary Surfaces: Application to Meridiani Planum, Mars. *Journal of Geophysical Research: Planets*, 111 (E12), E12S02-. <http://dx.doi.org/10.1029/2005JE002544>

This paper is posted at ScholarlyCommons. [http://repository.upenn.edu/ees\\_papers/82](http://repository.upenn.edu/ees_papers/82)  
For more information, please contact [libraryrepository@pobox.upenn.edu](mailto:libraryrepository@pobox.upenn.edu).

---

# Spatial Grain Size Sorting in Eolian Ripples and Estimation of Wind Conditions on Planetary Surfaces: Application to Meridiani Planum, Mars

## **Abstract**

The landscape seen by the Mars Exploration Rover (MER) Opportunity at Meridiani Planum is dominated by eolian (wind-blown) ripples with concentrated surface lags of hematitic spherules and fragments. These ripples exhibit profound spatial grain size sorting, with well-sorted coarse-grained crests and poorly sorted, generally finer-grained troughs. These ripples were the most common bed form encountered by Opportunity in its traverse from Eagle Crater to Endurance Crater. Field measurements from White Sands National Monument, New Mexico, show that such coarse-grained ripples form by the different transport modes of coarse- and fine-grain fractions. On the basis of our field study, and simple theoretical and experimental considerations, we show how surface deposits of coarse-grained ripples can be used to place tight constraints on formative wind conditions on planetary surfaces. Activation of Meridiani Planum coarse-grained ripples requires a wind velocity of 70 m/s (at a reference elevation of 1 m above the bed). From images by the Mars Orbiter Camera (MOC) of reversing dust streaks, we estimate that modern surface winds reach a velocity of at least 40 m/s and hence may occasionally activate these ripples. The presence of hematite at Meridiani Planum is ultimately related to formation of concretions during aqueous diagenesis in groundwater environments; however, the eolian concentration of these durable particles may have led to the recognition from orbit of this environmentally significant landing site.

## **Keywords**

grain, Mars, ripples

## **Disciplines**

Earth Sciences | Environmental Sciences | Physical Processes | Physical Sciences and Mathematics | Sedimentology

# Spatial grain size sorting in eolian ripples and estimation of wind conditions on planetary surfaces: Application to Meridiani Planum, Mars

Douglas J. Jerolmack,<sup>1</sup> David Mohrig,<sup>1</sup> John P. Grotzinger,<sup>1,2</sup> David A. Fike,<sup>1</sup> and Wesley A. Watters<sup>1</sup>

Received 27 July 2005; revised 17 November 2005; accepted 29 November 2005; published 27 May 2006.

[1] The landscape seen by the Mars Exploration Rover (MER) Opportunity at Meridiani Planum is dominated by eolian (wind-blown) ripples with concentrated surface lags of hematitic spherules and fragments. These ripples exhibit profound spatial grain size sorting, with well-sorted coarse-grained crests and poorly sorted, generally finer-grained troughs. These ripples were the most common bed form encountered by Opportunity in its traverse from Eagle Crater to Endurance Crater. Field measurements from White Sands National Monument, New Mexico, show that such coarse-grained ripples form by the different transport modes of coarse- and fine-grain fractions. On the basis of our field study, and simple theoretical and experimental considerations, we show how surface deposits of coarse-grained ripples can be used to place tight constraints on formative wind conditions on planetary surfaces. Activation of Meridiani Planum coarse-grained ripples requires a wind velocity of 70 m/s (at a reference elevation of 1 m above the bed). From images by the Mars Orbiter Camera (MOC) of reversing dust streaks, we estimate that modern surface winds reach a velocity of at least 40 m/s and hence may occasionally activate these ripples. The presence of hematite at Meridiani Planum is ultimately related to formation of concretions during aqueous diagenesis in groundwater environments; however, the eolian concentration of these durable particles may have led to the recognition from orbit of this environmentally significant landing site.

**Citation:** Jerolmack, D. J., D. Mohrig, J. P. Grotzinger, D. A. Fike, and W. A. Watters (2006), Spatial grain size sorting in eolian ripples and estimation of wind conditions on planetary surfaces: Application to Meridiani Planum, Mars, *J. Geophys. Res.*, *111*, E12S02, doi:10.1029/2005JE002544.

## 1. Introduction

[2] The primary objective of the Mars Exploration Rovers (MER) mission is to seek out evidence regarding the history of water on the Martian surface [Squyres *et al.*, 2003]. The landing site at Meridiani Planum was chosen because of gray/crystalline hematite detected there by the Mars Global Surveyor (MGS) Thermal Emission Spectrometer (TES), which was interpreted to reflect iron precipitation in surficial aqueous environments [Christensen *et al.*, 2000; Golombek *et al.*, 2003]. After landing, data from the rover Opportunity confirmed the presence of hematite [Christensen *et al.*, 2004; Klingelhofer *et al.*, 2004; Squyres *et al.*, 2004], which is interpreted to have formed in an aqueous diagenetic environment, as expressed principally by hematite-enriched concretions scattered throughout the outcrop [McLennan *et al.*, 2005]. As important as aqueous

diagenesis was in precipitating hematite at Meridiani, the direct analysis of bedrock by Opportunity's miniTES provides only a subtle spectral response for hematite [Christensen *et al.*, 2004]. Instead, the enrichment required to produce the strong spectral response for hematite as seen by TES from orbit is likely to have been caused by erosion of bedrock and concentration of hematitic concretions and their fragments as a lag deposit [Soderblom *et al.*, 2004].

[3] Opportunity's trek between Eagle and Endurance craters reveals that the concentration of hematitic concretions and concretion fragments may not just be the result of simple deflation; rather, these particles appear to form discrete bed forms, suggesting that lateral transport has been an additional, or even dominant, factor in their spatial sorting [Sullivan *et al.*, 2005]. Further motivation to constrain the styles and magnitudes of Martian eolian processes is provided by the general recognition that wind-related transport has been one of the most active geomorphic agents on the surface of Mars [Sagan and Bagnold, 1975; Greeley and Iversen, 1985]. At the Opportunity landing site, wind-driven transport of particles has acted to erase crater rims, fill in crater floors with loose sediment, and sculpt bedrock exposures via sand blasting [Soderblom *et al.*, 2004;

<sup>1</sup>Department of Earth, Atmospheric and Planetary Sciences, Massachusetts Institute of Technology, Cambridge, Massachusetts, USA.

<sup>2</sup>Now at Geological and Planetary Sciences, California Institute of Technology, Pasadena, California, USA.

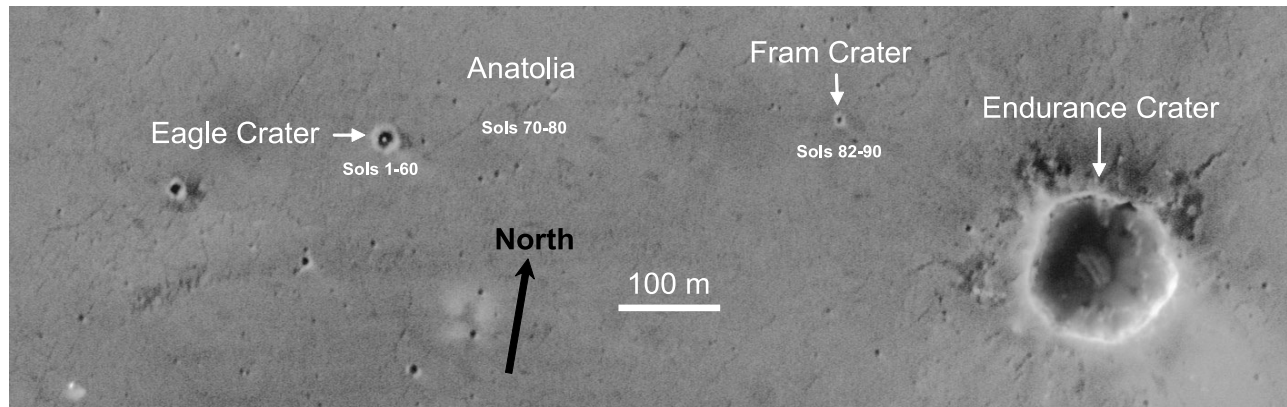


**Figure 1.** MOC image (R1602188) of Meridiani Planum showing the study area. Labels indicate the approximate range of sols spent at each location on the traverse of Opportunity from Eagle Crater to Endurance Crater.

*Sullivan et al.*, 2005]. Additionally, the stratigraphy observed in sedimentary rocks is interpreted as preserving a record of ancient eolian processes that must be separated from stratigraphy produced by flowing water to accurately reconstruct depositional environments [*Squyres et al.*, 2004; *Grotzinger et al.*, 2005].

## 2. Background

[4] For this study we examine eolian features observed by Opportunity during its traverse from Eagle to Endurance Crater, collected over a period of approximately 40 Martian days (sols, which equal 24.67 Earth hours, where Sol 1 is 24 January 2004) during the first half of year 2004 (Figure 1). All images used are in the public domain and freely available on the Internet (<http://marsrovers.jpl.nasa.gov/gallery/all/opportunity.html>). At the Opportunity landing site on Meridiani Planum, loose sediment has been worked by wind into one of three forms distinguished by grain size and sorting. The finest deposits are dust streaks forming in the lees of topographic obstacles on the plains surface [*Sullivan et al.*, 2005]. Intermediate forms are well-sorted ripples consisting of fine and medium sand of basaltic composition that accumulates locally in depressions [*Sullivan et al.*, 2005], where the composition of these grains has been interpreted using the MiniTES [Christensen *et al.*, 2004; Soderblom *et al.*, 2004]. The coarsest-grained topography is ripples enriched in hematitic particles (Figure 2) [*Soderblom et al.*, 2004; *Sullivan et al.*, 2005]. The Mössbauer instrument has been used to determine the nature of these grains [*Klingelhofer et al.*, 2004], however their composition is uncertain and they may contain a significant fraction of basalt [*McLennan et al.*, 2005]. Although the grain density values used in our sediment transport formulations are estimated from (uncertain) clast mineralogical composition, the calculations are not very sensitive to grain density and thus uncertainties in grain composition will not affect the main conclusions of this paper.

[5] Wind transport has acted to concentrate fragments of hematitic spherules on the surface of ripple crests covering the plains of the Opportunity landing site. Here we focus on the environmental conditions necessary to form these

hematite-rich ripples. These ripples differ from more common eolian features by having crests made up of very large grains while troughs consist of much finer material (see section 3.5). Their ubiquity on Meridiani Planum makes quantitative interpretation of their formative conditions particularly relevant to assessing the dominant processes that have sculpted the surface in the past and those that are active today. Because Opportunity has not recorded any motion of these ripples, the environmental conditions can be estimated only from properties of the bed forms themselves. A central question is, “How different are these conditions from present windiness, and how long has it been since the coarse-grained ripples were last active?”

[6] In order to confirm or modify the hypothesized mechanisms of coarse-grained ripple formation developed by earlier workers [*Bagnold*, 1941; *Sharp*, 1963; *Ellwood et al.*, 1975; *Fryberger et al.*, 1992], we collected measurements at White Sands National Monument, New Mexico, USA. These data define the sediment flux, grain size, wind speed, ripple morphology and ripple migration rate, and confirm that the spatial sorting in grain size that characterizes these ripples arises from different modes of transport for different grain size fractions. We then develop a method for using grain size differences between the ripple crests and troughs to estimate transport conditions that can be related to wind properties. Microscopic Imager (MI) images from Opportunity provide previously unavailable grain size data (Figure 2), allowing application of our method to estimate wind speeds at Meridiani Planum during the time of ripple formation. In addition, images from Opportunity’s Panoramic camera (Pancam) and Navigation camera (Navcam) provide important morphological information and context (Figure 2).

[7] The method reported here should in principle be applicable to Mars, Earth, and any planet where eolian deposits are present and sufficient data are available. The main results using data collected with Opportunity are estimates of minimum and maximum wind speeds that shaped the present Meridiani Plains at the landing site. Time-sequence orbital images from the Mars Orbiter Camera (MOC) of dust streaks at Meridiani Planum that have reversed direction (Figure 3) [*Sullivan et al.*, 2005] are used to estimate the minimum speed of modern surface winds (1997 to present) during dust-clearing events. We find that

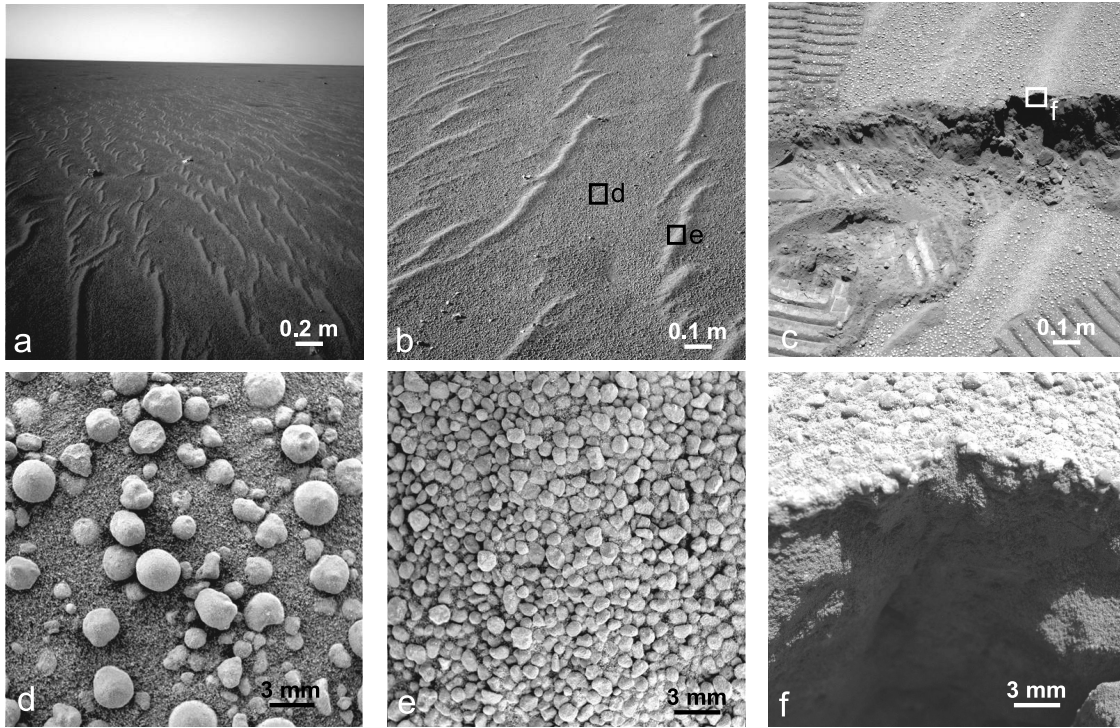


**Figure 2.** Coarse-grained ripples at Meridiani. (a) Navcam image (1N135566467EFF1300P1981R0M1, sol 83) of Meridiani Planum near Anatolia. (b) Pancam image (1P136100316EFF1500P2436R1M1, sol 89) showing typical coarse-grained ripples, where boxes show regions exemplified in Figures 2d and 2e. (c) Pancam image (1P135374557EFF10CIP2421L7M1, sol 81) showing exposed trench dug by Rover wheel. Box shows location of Figure 2f. (d) MI image (1M135284483EFF10CGP2956M2M1, sol 80) of typical inter-ripple zone showing hematitic spherules and fragments, and basaltic sand matrix. (e) MI image of typical coarse-grained ripple crest (1M134664602EFF1000P2936M2M1, sol 73) showing monolayer of hematitic fragments. (f) MI image (1M135284929EFF10CGP2956M2M1, sol 80) of ripple trench shown in Figure 2c.

this estimated wind velocity is greater than one half of the wind velocity necessary to initiate motion of coarse-grained plains ripples, and from this we infer that the present-day surface may have been active recently.

### 3. Theory and Methods

[8] Knowledge of the boundary shear stress, a fluid property, and critical shear stress and settling velocity, both grain properties for a given fluid, is necessary for elementary calculations of sediment transporting conditions and sediment flux estimates. The critical shear stress is the boundary shear stress exerted by the fluid on the bed that is required to initiate grain motion, while the settling velocity is the terminal fall velocity of a grain. The magnitudes for each of these grain parameters depend on fluid density and viscosity, and we can explicitly account for these properties so that universal expressions can be derived and applied to Earth and Mars. In this section we describe these parameters in detail and show how they can be used to characterize modes of sediment transport.

#### 3.1. Fluid Shear Velocity

[9] Flow of a viscous fluid over a granular bed imparts a shear stress to the surface, called the boundary shear stress,  $\tau$ , which is the fundamental property of the flow used to

parameterize the associated sediment transport. It is convenient to define wind strength in terms of the mean shear velocity,  $u_*$ , where

$$\tau = \rho_f u_*^2, \quad (1)$$

and  $\rho_f$  is fluid density. From (1) it is clear that the surface stress imparted by a wind on Mars will be less than a wind of the same shear velocity on Earth, because the density of the modern Martian atmosphere is much less (Table 1). In terms of sediment transport, some of this effect is offset by the lower stress required to move grains on Mars because of its reduced gravity. Velocity profiles in turbulent boundary layers developing on a flat bed under approximately steady and uniform conditions (i.e., constant in space and time) are known to exhibit a logarithmic form,

$$u(z) = \frac{u_*}{\kappa} \ln\left(\frac{z}{z_0}\right), \quad (2)$$

where  $u(z)$  is the time-averaged wind velocity as a function of elevation above the bed,  $z$ ,  $\kappa$  is von Kármán's constant and is equal to 0.4, and  $z_0$  is a roughness parameter, equal to the elevation at which the extrapolated logarithmic velocity profile goes to zero (Figure 4). When

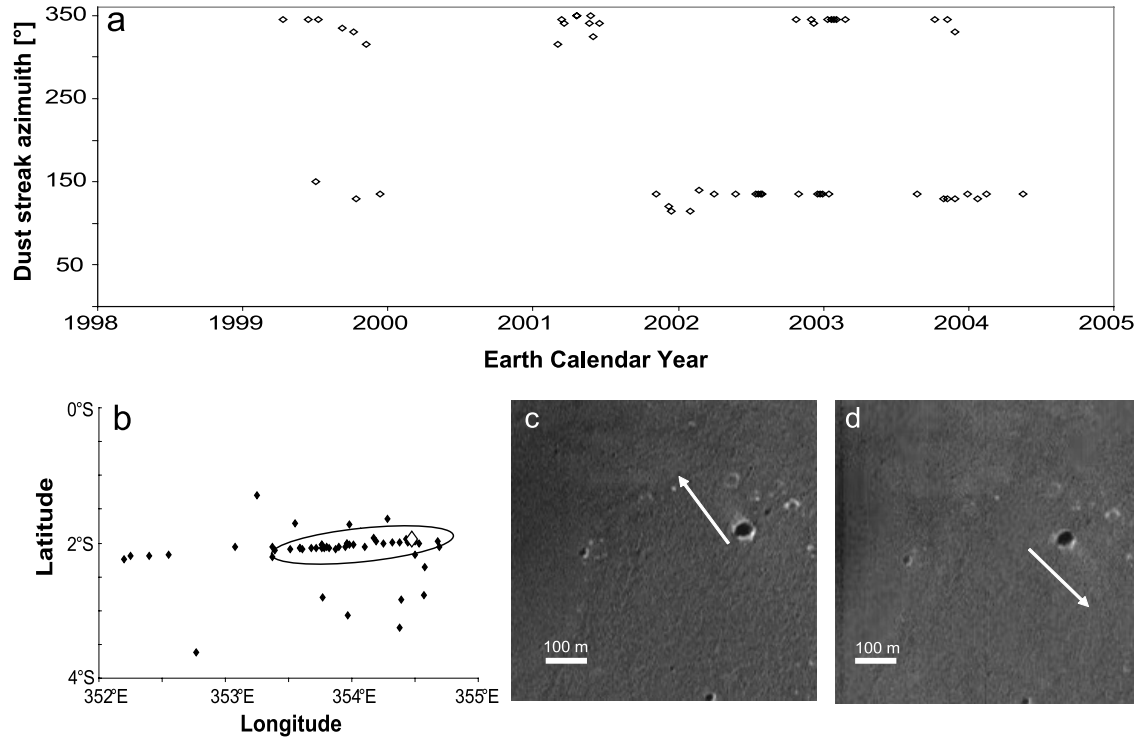


**Figure 3.** Reversing dust streaks at Opportunity landing site. (a) Measured orientation in degrees azimuth of all dust streaks observed in the vicinity of the Opportunity landing ellipse, and times associated with each image. Note alternating direction of predominant dust streak orientation with time. (b) Locations of all images analyzed in this study, with the Opportunity landing ellipse shown for reference. Large open diamond marks actual Opportunity landing site in Eagle Crater. (c, d) MOC images (E0200373 and E1800855, respectively) showing a dust streak that has reversed direction. Arrows indicate orientation of dust streaks.

measurements of the velocity profile are present, the magnitude of  $u_*$  can be determined using (2) (Figure 4). Owing to the large density contrast between sand grains and air, both on Earth and on Mars, turbulent velocity fluctuations do not strongly influence sediment transport and hence mean velocity values are appropriate (see Appendix A and Lee [1987]).

### 3.2. Grain Settling Velocity

[10] Settling velocity,  $w_s$ , can be calculated using a variety of empirical expressions, which differ in the formulation of the drag coefficient as a function of fluid and grain properties. A simple expression found to perform well for a variety of particles [Ferguson and Church, 2004] is

$$w_s = \frac{(s-1)gd^2}{C_1\nu + (0.75C_2(s-1)gd^3)^{1/2}}, \quad (3)$$

where  $s = \rho_s/\rho_f$  is the relative density of sediment,  $\rho_s$  is sediment density,  $g$  is acceleration due to gravity,  $\nu$  is kinematic viscosity (Table 1),  $d$  is grain diameter,  $C_1$  is a constant with a theoretical value of 18, and  $C_2$  is the constant asymptotic value of the drag coefficient (equal to 1 for typical natural grains).

### 3.3. Threshold of Motion

[11] Bagnold [1941] observed two threshold shear velocity values for wind-blown sand: the fluid (critical) threshold for initiation of motion for static grains,  $u_{*c}$ , and the

dynamic (impact) threshold,  $u_{*i}$ , which is the shear velocity required to sustain particle motion. The shear velocity required to sustain particle motion is lower than that to initiate motion because once particles begin to move, their quasi-elastic collisions with stationary grains on the bed transfer momentum to the bed particles. It has been found experimentally that  $u_{*i} \approx 0.7 u_{*c}$  [Bagnold, 1941; Nishimura and Hunt, 2000].

[12] Sagan and Bagnold [1975] were the first to estimate the wind-blown threshold-of-motion for Mars, by applying dimensional analysis to data from subaqueous flume experiments on Earth. Iversen and White [1982] carried out an important set of experiments defining the initiation of motion for grains having a wide range of size, density and shape (from very angular crushed walnut shells to rounded quartz sand), in gas of varying density. They combined their results with previous measurements to derive a threshold-of-motion curve with atmospheric pressures ranging from Martian to Venusian conditions. Several authors have fitted

**Table 1.** Relevant Physical Parameters for Mars and Earth

	$\nu$ , m <sup>2</sup> /s	$\rho_f$ , kg/m <sup>3</sup>	$g$ , m/s <sup>2</sup>
Mars <sup>a</sup>	$6.35 \times 10^{-4}$	0.02	3.72
Earth <sup>b</sup>	$0.32 \times 10^{-4}$	1.23	9.81

<sup>a</sup>Martian atmospheric kinematic viscosity and density assume air temperature of 240 K, surface pressure of 5 mb, and an atmospheric composition of 100% CO<sub>2</sub> [Pollack et al., 1976].

<sup>b</sup>Earth values are at sea level assuming air temperature of 293 K.

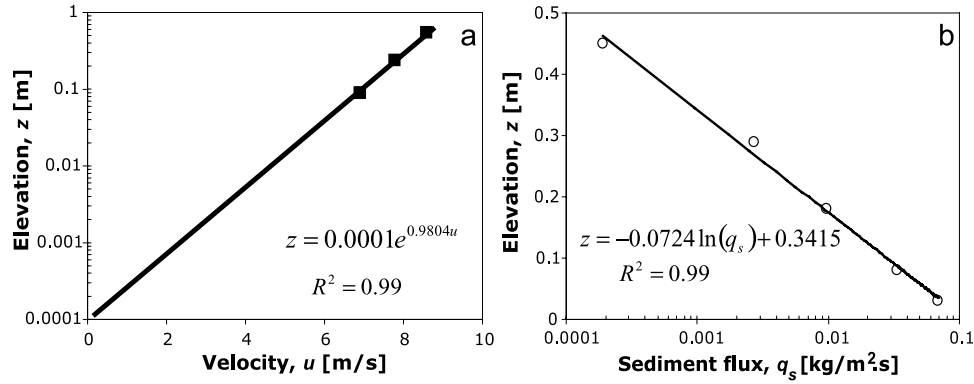


**Figure 4.** Data collected over coarse-grained ripples at White Sands. Note that although elevation,  $z$ , is the independent variable, it is plotted on the  $y$  axis here to generate profiles. (a) Wind velocity profile plotted in linear-log space. Solid line is a best fit exponential function (fit is logarithmic if  $z$  is plotted on  $x$  axis), extrapolated to zero velocity where the elevation intercept defines the roughness parameter,  $z_0 \approx 10^{-4}$  m. Shear velocity is estimated from best fit line using equation (2). (b) Horizontal saltation mass flux profile measured using box samplers, plotted in log linear space. Solid line is a best fit logarithmic function (fit is exponential if  $z$  is plotted on  $x$  axis). Total saltation flux was obtained by integrating the mass flux profile from  $z = 0$  m to  $z = 0.45$  m.

explicit functions to these data; the expression by *Shao and Lu* [2000] provides a reasonable compromise between simplicity and accuracy,

$$u_{*c} = \sqrt{0.0123 \left( sgd + \frac{3.0 \times 10^{-4} \text{ kg/s}^2}{\rho_f d} \right)}. \quad (4)$$

[13] Equation (4) was derived from a fit of *Iversen and White's* [1982] data over the range  $0.05 \leq d \leq 1.8$  mm, where  $d$  is the nominal grain diameter. Cohesion between grains, due to electrostatic forces, moisture content and other effects, becomes significant when particle surface area is large compared to particle volume (i.e., for small grains) [*Iversen and White*, 1982; *Shao and Lu*, 2000; *Cornelis and Gabriels*, 2004]. The effects of cohesion on Mars are not well constrained, and consequently the predicted threshold of motion values from various authors diverge for grain sizes smaller than 0.1 mm [*Sagan and Bagnold*, 1975; *Miller and Komar*, 1977; *Iversen and White*, 1982; *Greeley and Iversen*, 1985]. It is clear, however, that because of cohesion effects the aerodynamic entrainment of very fine grains (such as Martian dust with median grain diameter,  $d_{50} < 0.01$  mm [*White et al.*, 1997; *Greeley et al.*, 2000]) requires a larger shear velocity than entrainment of fine sand (e.g.,  $d = 0.1$  mm).

[14] Care must be taken in using calculated threshold of motion values to infer threshold conditions for specific size fractions within sediment mixtures. *Wiberg and Smith* [1987] showed that for heterogeneous sediment transport,  $u_{*c}$  for a specific size class depends on the ratio of the representative grain diameter of that size class to the grain diameter of the representative particle size composing the bed. For example, large grains on a bed composed primarily of fines are more exposed and hence more susceptible to transport. Data from *Fenton and Abbot* [1977] and *Fisher et al.* [1983], together with the analysis of *Wiberg and Smith* [1987] indicate that a “perched” grain with diameter

5 times larger than the diameter of the grains which comprise the bed has a critical shear velocity that is reduced by a factor of  $\sqrt{6}$  compared to the necessary shear velocity for the case where the same grain rests on a bed of particles of the same size. Further, even sparse coverage of coarse sediment inhibits the transport of finer grains, because the larger grains extract momentum from the flow [*Gillette and Stockton*, 1989; *Nickling and McKenna Neuman*, 1995]. In this way, surface coarsening of mixed sediment via selective transport and removal of finer particles can proceed until the coarse particles are sufficiently concentrated that they act to stabilize the bed [*Bagnold*, 1941; *Chepil*, 1945; *Gillette and Stockton*, 1989].

### 3.4. Modes of Transport

[15] Having defined the crucial parameters for characterizing sediment transport, namely  $u_*$  (1),  $u_{*c}$  (4) and  $w_s$  (3), we can now discuss the movement of sediment and its characterization by use of these parameters. *Bagnold* [1941] recognized three modes of wind-blown sediment transport: saltation, creep and suspension. If the shear stress of the wind exceeds the critical value for initiation of motion of grains then saltation may occur, in which the grains hop with skewed parabolic (ballistic) trajectories in between semi-elastic collisions with the bed (Figure 5a) (for theoretical and numerical treatments see, e.g., *Anderson and Haff* [1988] and *Nalpanis et al.* [1993]). Grains traveling purely in saltation are little affected by turbulent fluctuations in wind velocity near the bed. Saltating particles impart approximately half of their kinetic energy to grains on the bed, dislodging other grains that can either “splash” short distances (reptation), or can themselves be ejected higher into the flow, becoming part of the saltation layer (Figure 5) [*Anderson and Haff*, 1988]. It has been observed that the impact of a saltating grain can dislodge up to ten grains via splash [*Bagnold*, 1941; *Anderson and Haff*, 1988].

[16] Creep consists of particles that are too heavy to be transported directly by the wind drag and lift acting on them

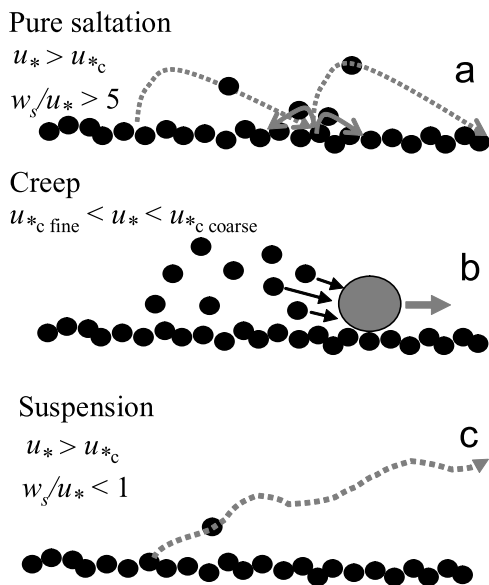


**Figure 5.** Modes of eolian sediment transport. (a) Saltation, where dotted lines show typical ballistic trajectory of a saltating particle, and solid lines show grain splash, or reptation trajectories. (b) Creep, in which the large grain moves close to the ground owing to combination of collisions by finer saltating cloud and fluid drag. (c) Suspension, in which the grain is lofted by fluid turbulence and advected far into the air before returning to the bed.

at a given wind speed, but can move when these fluid-imparted forces are combined with collisions from incoming saltating particles [Bagnold, 1941; Fryberger *et al.*, 1992]; grains in creep move close to the bed. Because of the collisional component driving their motion, grains transported in creep move at values for  $u^*$  that are smaller than  $u_{*c}$  associated with purely wind-driven transport [Bagnold, 1941; Fryberger *et al.*, 1992]. Saltating grains impacting the bed can drive surface creep of particles that are 6 times larger [Bagnold, 1941]. If wind shear velocity increases to become larger than  $u_{*c}$  for grains in creep, these grains will travel in saltation as described above.

[17] Particles with settling velocities that are small compared to upward-directed turbulent wind velocities for a given wind condition can be lifted high into the fluid and advected long distances between contact with the bed. These grains are considered to be traveling in suspension (Figure 5). We define dust in this paper as grains that are small enough that they are entrained directly into suspension when wind exceeds the critical shear velocity (as in the work of Shao [2000]). In reality, the transitions between creep and saltation or saltation and suspension are gradual [Walker and Southard, 1984; Nickling, 1983; Nishimura and Hunt, 2000; Niño *et al.*, 2003], and defining the exact nature of particle trajectories is a subject of vigorous research [Walker and Southard, 1984; Anderson and Haff, 1988; Nalpanis *et al.*, 1993; Nishimura and Hunt, 2000]. Although suspended-sediment transport is not explicitly considered in our analysis of ripples at Meridiani and White Sands, characterization of suspension is important for many applications and is included here for completeness (see Appendix A).

[18] The magnitude of vertical velocity fluctuations scales with shear velocity in steady and uniform turbulent boundary layer-flow [see Bagnold, 1966; Niño *et al.*, 2003]. The ratio  $w_s/u_*$ , then, characterizes the balance between downward settling of particles and their transport into the interior of the flow via turbulent fluctuations in vertical velocity. Observations in air [Bagnold, 1941; Chepil, 1945; Bagnold, 1966; Gillette and Goodwin, 1974; Sagan and Bagnold, 1975; Nishimura and Hunt, 2000; Shao, 2000] and underwater [e.g., Niño *et al.*, 2003] have empirically related transport style to  $w_s/u_*$ , with the following general results (for  $u_* > u_{*c}$ ),

$$w_s/u_* < 1 \quad \text{suspension} \quad (5a)$$

$$w_s/u_* > 5 \quad \text{pure saltation.} \quad (5b)$$

Condition (5a) has been debated by many authors (since Bagnold [1966]) because the transition to suspension is gradual and defining it is subjective. There is as yet, however, no reason to expect that the transition to suspension should occur for different values of  $w_s/u_*$  in the Martian atmosphere as compared to Earth (see Appendix A). Pure saltation (5b) consists of ballistic trajectories of grains as described above (Figure 5). There is a gradual transition from saltation to suspension [Nishimura and Hunt, 2000; Niño *et al.*, 2003], in which fluid turbulence effects are measurable but do not dominate particle trajectories. We have seen above (equation (3)) that settling velocity increases with grain size. If a bed of mixed grain sizes is subject to a given shear velocity,  $u_*$ , the smallest grains may travel by suspension (and hence leave the area of interest), while larger grains may travel by pure or modified saltation. For even larger grains, for which  $u_* < u_{*c}$ , the grains may not move at all, or may be driven only by creep (Figure 5). In this manner, the wind can spatially sort grains on an initially well-mixed bed (Figure 6), and by using grain size data along with equations (3), (4) and (5a) we can deduce the range of  $u_*$  that generated the observed surface. This technique is applied in section 4.

### 3.5. Bed Form Morphology

[19] In terrestrial eolian environments the term ripple generally refers to a bed form whose wavelength is determined by the characteristic path length of sand grains in transport, and this wavelength is less than a few meters [Bagnold, 1941; Ellwood *et al.*, 1975; Anderson and Bunas, 1993]. Eolian ripples can be separated into two groups depending on the sorting of particles making up the bed form. In the first group there is little difference in the distribution of particles composing the ripple crests and the distribution of particles composing the ripple troughs (Figure 6a). Ripples in this group, sometimes called “splash ripples” [e.g., Anderson and Bunas, 1993], are the most commonly observed forms and have been shown to be constructed from grains splashed by saltation [Bagnold, 1941; Sharp, 1963; Ellwood *et al.*, 1975; Anderson and Bunas, 1993]. The second group of ripples is characterized by a large difference in the size of grains making up the crestal portions of ripples and grains covering the troughs of ripples (Figure 6b), which is usually due to an initially



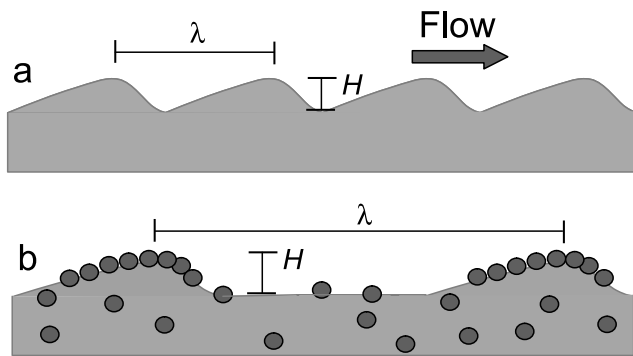


**Figure 6.** Schematic cross section showing profile and subsurface composition of two basic ripple types. Ripple wavelength,  $\lambda$ , ripple height,  $H$ , and wind direction are indicated. (a) Splash ripples. (b) Coarse-grained ripples. No attempt is made to represent stratigraphy.

bimodal distribution of grain size of the source sediments. The diameter of the crestal grains is generally substantially greater than that of grains in the troughs. We will refer to these spatially sorted ripples simply as coarse-grained ripples. Previous authors have described similar features as “granule ripples” [e.g., Sharp, 1963] or “mega-ripples” [e.g., Greeley and Iversen, 1985], however we believe the term “coarse-grained ripples” is more general because the term ‘granule’ refers specifically to particles with a diameter of 2 mm and larger, while mega-ripple implies an unusually large ripple size which is not necessarily the case. These ripple forms have been studied by a number of investigators [Bagnold, 1941; Sharp, 1963; Ellwood *et al.*, 1975; Fryberger *et al.*, 1992], all of whom suggest that development of this topography is the product of saltating and creeping grains. It has been proposed that the spatial sorting within the ripples is an expression of particles moving via the different transport styles and with different particle excursion lengths [Ellwood *et al.*, 1975]. The barely mobile coarse grains have been observed to cluster on the surface when they collide with other grains of similar size [Bagnold, 1941; Fryberger *et al.*, 1992], and these coarse grains protect the underlying fine grains from being transported by wind. In this manner, the clusters of coarse grains become ripple crests.

[20] It has been observed that terrestrial splash ripples have characteristic wavelengths that are smaller than those associated with coarse-grained ripples (Figure 6), but the relationships between grain size, wind speed, and bed form wavelength and height are incompletely understood [Bagnold, 1941; Sharp, 1963; Ellwood *et al.*, 1975; Fryberger *et al.*, 1992; Anderson and Bunas, 1993]. Presently, ripple geometry cannot be used quantitatively to place constraints on formative wind conditions, and hence we will use morphological data only as a qualitative guide in ripple interpretation. In contrast, grain size data do permit a quantitative reconstruction of wind speed.

#### 4. Observations of Eolian Features

[21] We focus on coarse-grained ripples and how data from them can be used to quantitatively constrain environmental conditions shaping the Meridiani Plains at the

Opportunity landing site. Our method for estimating environmental conditions using these ripples is based in part on previous studies of terrestrial coarse-grained ripples. In addition, we have obtained data at White Sands National Monument, New Mexico, USA, demonstrating the connection between different styles of sediment transport and development of spatial size sorting of particles composing coarse-grained ripples.

##### 4.1. Eolian Features at the Opportunity Landing Site, Meridiani Planum

[22] Coarse-grained ripples with wavelengths of 0.5–1 m and amplitude of about 10 mm (Figure 2) were the most common feature seen by Opportunity on the traverse from Eagle Crater to Endurance Crater [Soderblom *et al.*, 2004]. The crests are composed of very uniform, subrounded grains (using scale of Powers [1953]) of very coarse sand (Figure 2e). A trench dug by the Rover wheel through a ripple crest (Figure 2f) reveals that the coarse grains reside only on the surface, forming a monolayer. We assume these hematitic clasts [Klingelhofer *et al.*, 2004; McLennan *et al.*, 2005] have a density of  $\rho_s = 4100 \text{ kg/m}^3$ , a value used by Sullivan *et al.* [2005] that lies in the middle of a previously estimated density range [McLennan *et al.*, 2005]. Our results will not be strongly affected by the choice of grain density. The crestal grains are interpreted to be fragments of larger hematitic spherules broken up by transport processes [Soderblom *et al.*, 2004]. This interpretation is consistent with the chipped and frosted (whitened) appearance of spherules on the plains (Figure 2d), indicating that the spherules have been altered by transport. The interior of the ripple crest is composed of fine-grained sand that is primarily basaltic [Soderblom *et al.*, 2004], with an assumed density of  $\rho_s = 3000 \text{ kg/m}^3$ . We cannot resolve the grain size distribution of these small particles, because they only occupy several pixels in MI images (which have a resolution of  $\sim 0.03 \text{ mm/pixel}$  [Herkenhoff *et al.*, 2003]) and are generally not distinct enough to confidently measure, but the size range appears to be 0.05–0.2 mm.

[23] The troughs between ripple crests contain a mixture of hematitic spherules up to 5 mm in diameter [Christensen *et al.*, 2004; Klingelhofer *et al.*, 2004; Soderblom *et al.*, 2004], spherule fragments and a finer-grained basaltic sand matrix (Figure 2d) [Sullivan *et al.*, 2005] of similar composition to ripple-crest interiors. In contrast to more familiar ripples composed of a unimodal distribution of grains that resemble a continuous train of skewed sine waves, the morphology of coarse-grained ripples seen by Opportunity is characterized by small symmetric bumps separated by long flats (Figures 2 and 6). We will refer to these long flats generically as ripple troughs.

[24] The spatial sorting of grains between ripple crests and troughs is the most striking aspect of these features. We performed a grain size analysis of MI images obtained from the surfaces of three ripple crests and three ripple troughs along the traverse from Eagle Crater to Endurance Crater (Figure 7), following the grid-by-number sampling scheme [Wolman, 1954; Kellerhals and Bray, 1971]. In the analysis, a  $19 \times 19$  grid of evenly spaced points was laid over each image using ImageJ, a free image-processing software available online from the National Institutes of Health. The apparent long axis of each resolvable grain was

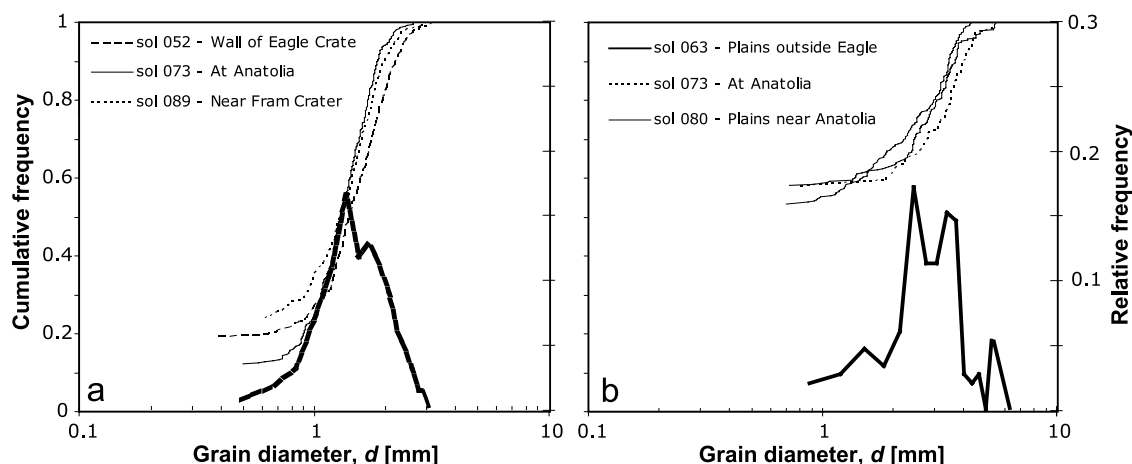


**Figure 7.** Cumulative grain size distributions and representative histograms for surface grains in Meridiani Planum MI grain counts; locations described in legends. (a) Coarse-grained ripple crests (1M132808584EFF06A8P2956M2M1, sol 52; 1M134664602EFF1000P2936M2M1, sol 73; 1M136083653EFF1500P2956M2M1, sol 89) and (b) ripple troughs (1M133776097EFF08A6P2957M2M1, sol 63; 1M134672134EFF1000P2936M2M1, sol 73; 1M135284423EFF10CGP2956M2M1, sol 80). Histograms are binned in 0.175-mm intervals, where relative frequency is number of measurements divided by total number of counted grains.

measured at every grid point, while unresolvable grains (specifically the finer basaltic grains) were counted as being less than 0.5 mm. Our cumulative grain size distributions were calculated using a total sample size of 361 points (Figure 7). Grain size distributions produced using this sampling method have been shown to be equivalent to grain size distributions generated by customary bulk-sieve analysis [Kellerhals and Bray, 1971; Kellerhals *et al.*, 1975]. The areal density of coarse grains (i.e., resolvable hematitic spherules and spherule fragments) in each image can be estimated by dividing the total number of counted resolvable grains by the number of grid points.

[25] Ripple crests (Figure 7a) show a surprisingly uniform grain size on all ripples (median grain size,  $d_{50} = 1.3$  mm), with no significant difference in distribution among them. Very little fine-grained cover is found on the ripple crests (Figure 2e), as verified by grain counts showing a coarse-grained coverage of greater than 75% for all ripple crests. Ripple troughs exhibit much poorer sorting than ripple crests (Figures 2d and 7b). Although the median grain diameter of the whole population cannot be computed, we can see from Figure 7b that it is slightly less than 1 mm. The median grain diameter will not be representative of this clearly bimodal population (in which the fines are missing from the plot). The coarser, resolvable grains have a fraction composed of hematitic fragments that are comparable to the ripple-crest population, and the balance are composed of intact spherules having a median diameter of about 3 mm. The areal density of coarse-grain coverage in ripple troughs has an average value of 44% (range of 42–47%).

[26] A final eolian feature at the Opportunity landing site that can be used to reconstruct wind conditions is bright dust streaks (Figure 3). These streaks, tapering away from crater rims, are composed of air fall dust deposited downwind of topographic obstacles such as crater rims, with an inferred grain size of less than 0.01 mm [Sullivan

*et al.*, 2005]. Images of particular craters show that dust streaks have been reoriented during the years 2001–2003 (Figure 3), providing direct evidence of sediment transport associated with high winds at Meridiani during this relatively short interval of observation. Further, our observations show that this lifting and redeposition of dust is a regional phenomenon. MOC images of all dust streaks in the vicinity of the Opportunity landing ellipse [Golombek *et al.*, 2003] over the period of 1997–2004 were used to estimate azimuth for each feature. A time series of dust-streak azimuth was generated from a total of 54 images. We find that there are two main orientations of dust streaks, and they are almost 180 degrees apart; these azimuths must correspond to the dominant wind direction associated with dust streak formation. The predominant orientation of regional dust streaks switched between these two azimuths at least twice over the observation period (Figure 3), and some observation periods show both orientations present. Taken together, the MOC image data show that winds at the surface of Meridiani Planum are presently strong enough to lift dust on the order of once a year.

#### 4.2. Terrestrial Ripples

[27] In order to quantify the transport processes of coarse-grained ripples and to verify hypotheses about their formation [Bagnold, 1941; Sharp, 1963; Ellwood *et al.*, 1975; Fryberger *et al.*, 1992], we conducted field experiments at White Sands National Monument, New Mexico, USA (Figure 8). The White Sands are a dune field made almost entirely of grains of gypsum which were eroded from evaporite deposits of Pleistocene Lake Otero (now dry) [McKee, 1966; Langford, 2003]. Our observations were collected during March 2004 over 3 days, when afternoon wind speeds were sufficient to mobilize all grain sizes present in the dune field. We observed coarse-grained ripples on the stoss (upwind) sides of many large dunes (Figure 9) along the “Heart of the Sands” dune trail. The

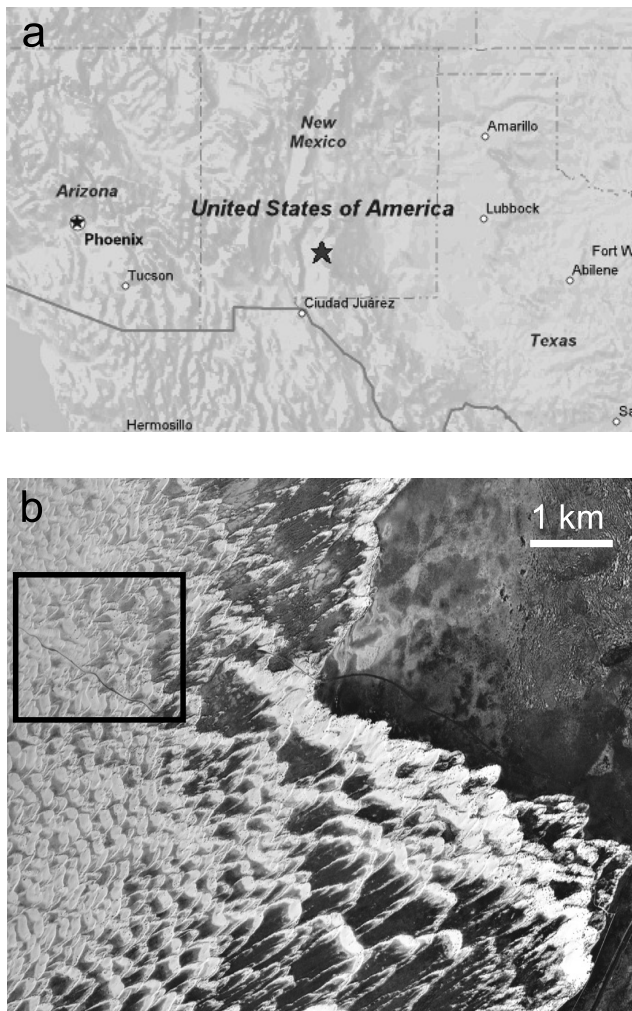


**Figure 8.** (a) Regional map of the United States with star indicating the location of White Sands National Monument. (b) Aerial photograph of the White Sands dune field (S. G. Fryberger, Geological overview of White Sands National Monument, 2005, available at <http://www.nps.gov/whsa/Geology%20of%20White%20Sands/GeoHome.html>); box indicates location of coarse-grained ripple observations near the “Heart of the Sands” dune trail.

occurrence of these ripples appeared to be related to the higher wind speeds present on dune backs, as compared to inter-dune depressions.

[28] These ripples had wavelengths of 0.5–1 m and heights,  $H \approx 10$  mm (Figures 6 and 9). Coarse grains were concentrated on the crests of ripples, while troughs contained few coarse grains (Figure 9). These large clasts were made of relatively dark rock fragments derived from Paleozoic and Precambrian granitic, siliclastic and carbonate rocks (S. G. Fryberger, Geological overview of White Sands National Monument, 2005, available at <http://www.nps.gov/whsa/Geology%20of%20White%20Sands/GeoHome.html>) exposed in outcrops upwind of the Lake Otero playa, and occurred only on the surface of the ripples (Figure 9c). The smaller grains making up ripple interiors and ripple troughs were composed of white gypsum (Figure 9). While some morphological features of these

ripples, such as their asymmetric shape, differ from the coarse-grained ripples observed at Meridiani Planum, the spatial segregation of relatively coarse and fine grain sizes at White Sands is very similar to the Martian examples.

[29] We measured wind speed, saltation flux, grain size, ripple size and ripple migration rates. These measurements were collected over many coarse-grained ripples during conditions when all particle sizes making up the bed were in motion.

[30] Wind velocity profiles were measured using three ultrasonic anemometers (Davis Wind Scribe, precision of 1%) placed 0.09 m, 0.24 m and 0.50 m above the bed. These instruments measured average and maximum wind speed for each 10-min observation interval. Shear velocity was calculated directly from the mean velocity readings using a least squares fit to equation (2) (Figure 4), and was equal to 0.41 m/s; this value is an average from four velocity profiles (range 0.40–0.43 m/s) and is used below in the analysis of sediment transport.

[31] The flux of sediment moving in saltation was measured using a stack of five sediment traps mounted on a vertical frame. These traps were designed and constructed by our research group and had a rectangular opening measuring 0.20 m wide and 0.05 m high, and a depth of 0.20 m. A screen having a mesh size of 0.125 mm was mounted at the back of each trap; grains having a smaller dimension were incompletely captured. The lowest trap was centered 0.04 m above the bed, with the higher traps spaced 0.04 m to 0.10 m apart (Figure 9f). The traps were tilted slightly in the vertical to avoid particle rebound and ejection from the back of the trap. Estimation of nominal grain diameters for all samples was performed using a Camsizer (Retsch Technology), which digitally images and measures most grains in a given sample. Thus errors associated with measuring grain size using this device are significantly less than sieve techniques and can be neglected. We measured the size distributions for grains transported in saltation at 0.04 m and 0.08 m above the bed, as well as for samples collected from the crests of ripples (Figure 9). Ripple crest samples were obtained with a scoop, and include material from both the ripple surface and ripple interior; no attempt was made to separate the two, rather the grain size distribution of the entire population was characterized.

[32] All saltating grains were gypsum in composition ( $\rho_s = 2380$  kg/m<sup>3</sup>) and ranged from less than 0.1 mm to 1 mm in diameter (Figure 10). Coarse-grained ripple crests were composed of two populations: gypsum particles having a size distribution similar to that collected in the saltation traps, and coarser rock fragments (measured  $\rho_s = 2630$  kg/m<sup>3</sup>) with diameters of 1–3 mm. (Figure 10). These coarser grains were not captured in the lowermost bin of our saltation sampler but were observed to be in motion very close to the bed. These coarse grains were found primarily on the surface of ripple crests and were much less common in ripple interiors (Figure 9c), however no quantitative information on this segregation was obtained.

[33] The horizontal sediment flux for each sediment trap was estimated by weighing the collected sample and dividing by its cross-sectional area and the observation time. These individual measures were then assembled to obtain a flux profile (Figure 4b). The total saltation flux,  $q_s$ , is

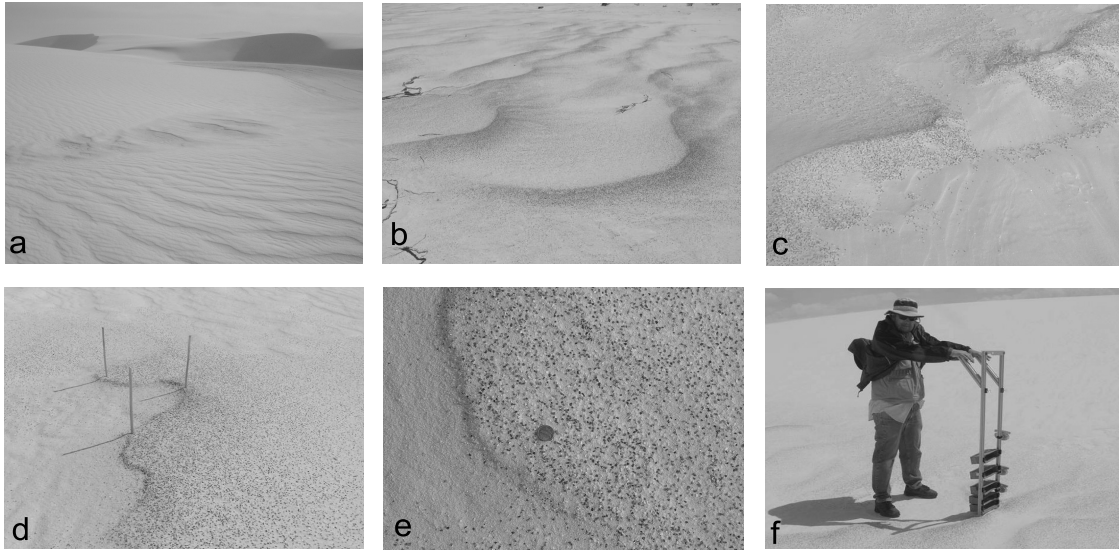


**Figure 9.** Coarse-grained ripples at White Sands National Monument. (a) Context view showing coarse-grained ripple train on the stoss side of a dune; wavelength between ripple crests about 1 m. (b) Closer view, where dark grains are siliciclastic granules on ripple crests; wavelength between crests about 1 m. (c) Ripple crest with coarse-grained layer removed to show finer-grained ripple interior; same scale as Figure 9b. (d) A ripple ( $\sim 10$  mm high) with stakes ( $\sim 0.2$  m high) for ripple migration observation. (e) Close-up of ripple crest showing coarse-grained surface layer; coin is  $\sim 20$  mm across. (f) The sediment sampler; ultrasonic anemometers are strapped to the far side of the frame.

defined as the mass per unit time per unit width transverse to the flow, and was calculated by integrating this profile of sediment flux (i.e., finding the area under the curve in Figure 4b); a representative value is  $8.0 \times 10^{-3} \text{ kg m}^{-1} \text{ s}^{-1}$  (range  $4 \times 10^{-3}$ – $11 \times 10^{-3} \text{ kg m}^{-1} \text{ s}^{-1}$ ). Although the trapping efficiency of our sampler is unknown, our measured saltation flux is similar to values reported by *Greeley et al.* [1996] for similar wind conditions. As a further check, we compare our measured flux to that predicted from the corrected *White* [1979] formula [see *Namikas and Sherman*, 1997],

$$q_s = 2.61 \frac{\rho_f u_*^3}{g} \left(1 - \frac{u_{*c}}{u_*}\right) \left(1 + \frac{u_{*c}}{u_*}\right)^2. \quad (6)$$

Using equation (6),  $q_s = 11 \times 10^{-3} \text{ kg m}^{-1} \text{ s}^{-1}$ , which is suitably close to the value obtained from our field measurements.

[34] The migration rate,  $c$ , of seven ripples was measured by placing 3–4 pins along the crestlines of each ripple (Figure 9d) and calculating average displacement of the crest over a 72-min interval. Mean ripple migration rate was 0.04 m/hr (range 0.02–0.08 m/hr). The amount of sediment moving in ripples is approximately equal to the creep mass flux [*Bagnold*, 1941],  $q_c$ , and can be estimated as

$$q_c = (1 - p)\rho_s c \frac{H}{2}, \quad (7)$$

where  $p$  is porosity and is assumed to be 0.4, and the ripple height  $H$  is defined in Figure 6. Our calculated creep mass flux is  $q_c = 0.09 \times 10^{-3} \text{ kg m}^{-1} \text{ s}^{-1}$  using  $c = 0.04$  m/hr,

$H = 10$  mm and  $\rho_s = 2630 \text{ kg/m}^3$  (grains in creep were rock fragments). Thus the creep flux was 2 orders of magnitude smaller than the saltation flux.

## 5. Interpretation and Discussion

### 5.1. Coarse-Grained Ripples at White Sands

[35] Our measurements over coarse-grained ripples at White Sands elucidate the mechanics of spatial grain size segregation in these bed forms. We calculated threshold shear velocity (equation (4)) and settling velocity (equation (3)) of gypsum and rock fragments over the observed size ranges; representative numbers are shown in Figure 11. Almost all grain sizes captured in the sediment traps had  $u_{*c}/u_* < 1$ ; that is, the observed shear velocity exceeded the threshold value for motion. Only the coarsest 2% of grains caught by traps had values for  $u_{*c}/u_*$  greater than 1, and all of these values were less than 1.2. The close agreement between the predicted and observed upper limit on saltation (Figure 11) is remarkable. Values of  $u_{*c}/u_*$  for the larger rock fragments were significantly greater than unity, and these grains moved only very close to the bed in creep (Figure 11). The spatial sorting associated with coarse-grained ripples is a direct result of different modes of transport for grains of different size and density; the gypsum grains all moved in saltation, while larger (and denser) rock fragments moved only in creep (Figures 10 and 11). Thus the genetic relationship between transport modes and coarse-grained ripples [*Bagnold*, 1941; *Sharp*, 1963; *Ellwood et al.*, 1975; *Fryberger et al.*, 1992] has been quantitatively verified through specific field measurements. Importantly, the flux of sediment moving in the ripples (creep flux) was two orders of magnitude less than the saltation flux. Hence the saltating

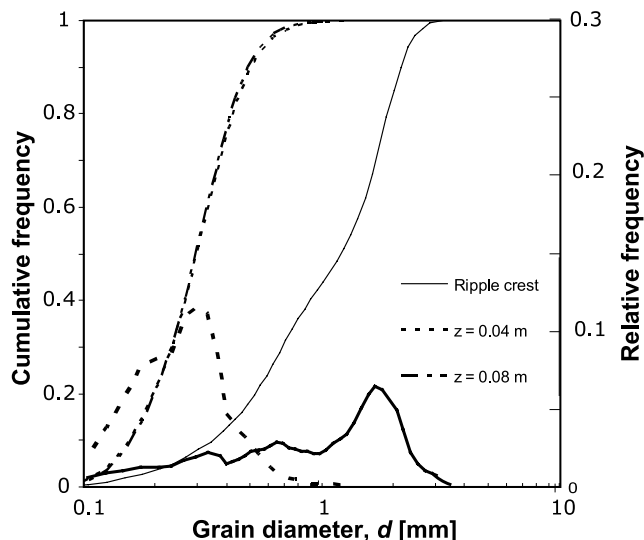


**Figure 10.** Cumulative weight grain size distributions and histograms from a coarse-grained ripple at White Sands, measured using a Camsizer. Particles were captured in saltation (0.04 m and 0.08 m above the bed), and in a grab sample from a ripple crest. Note that the ripple crest contains all grain sizes found in saltation (which are gypsum), plus a coarse fraction (rock fragments). All size distributions are generated by measuring more than  $10^5$  grains. Data are plotted from 47 binned grain size groups, where bin sizes are an increasing function of grain size and range from 0.01 mm to 0.35 mm.

population of grains was transported much more vigorously than the coarse grains making up the ripples, and this difference likely caused the observed sorting of White Sands coarse-grained ripples. This inference is supported by qualitative laboratory observations in which size segregation during the formation of coarse-grained ripples occurred owing to transport of larger grains in creep, while smaller grains moved in saltation [Bagnold, 1941; Fryberger *et al.*, 1992]

[36] We propose that the critical shear velocity for the creeping particles on a coarse-grained ripple crest can be used as an upper bound for wind conditions associated with their migration, as first suggested by Bagnold [1941]. If winds had moved all grains in these ripples in saltation, then the spatial grain sorting between crests and troughs would be suppressed, if not destroyed, because the characteristic transport lengths for all particles would be more similar than different [see Ellwood *et al.*, 1975]. Bagnold [1941] suggested that the minimum bound for creeping motion of grains is the impact threshold for the median diameter of grains in creep. For the White Sands ripples this diameter is 2 mm, and the corresponding minimum shear velocity is equal to  $0.7 u_{*c}$  [Bagnold, 1941; Nishimura and Hunt, 2000] or 0.50 m/s (5). This minimum shear velocity for creep coincides with the threshold shear velocity for the largest grains in saltation,  $u_{*c} = 0.49$  m/s. It is no simple coincidence that this estimated shear velocity is also very close to our measured wind shear velocity ( $u_* = 0.41$  m/s), and it supports Bagnold's [1941] hypothesis that, under most wind conditions, the shear velocity at the bed will be

approximately equal to the threshold condition of the coarsest grain fraction in motion.

## 5.2. Coarse-Grained Ripples at the Opportunity Landing Site, Meridiani Planum

[37] We propose that the coarse-grained ripples at the Opportunity landing site formed in a manner similar to those at White Sands, in which the hematitic fragments moved in creep while the fine-grained basaltic sand moved in saltation. Hematitic spherules were likely relatively immobile owing to their large size, and hence did not migrate to ripple crests. Ripple crest grains have a diameter 6 times that of the largest basaltic grains in ripple troughs, consistent with Bagnold's [1941] observation that saltating grains can drive creeping grains up to 6 times their size. The large spacing between ripple crests is also consistent with a coarse-grained ripple interpretation [Bagnold, 1941; Sharp, 1963; Ellwood *et al.*, 1975]. Results from White Sands, then, may be applied to resolve formative winds on the plains of Mars. The trench dug by Opportunity's wheel through a ripple crest (Figure 2) verifies that the surface of the plains has been coarsened via grain size selective transport by wind.

[38] We define here a reference velocity,  $u_{z=1}$ , which is the wind velocity at 1 m above the bed, for comparison of wind speeds. This requires an assumption of  $z_0$ , which is estimated here as  $k_s/30$  (valid for hydraulically rough boundary layer flows in any fluid), where  $k_s = 10$  mm is the ripple amplitude [e.g., Bagnold, 1941]. From (4) we calculate the maximum formative shear velocity of the Meridiani coarse-grained ripples to be 3.5 m/s ( $u_{z=1} = 70$  m/s), using  $u_{*c}$  for hematitic grains with a diameter of 1.3 mm. This is a maximum bound because a larger shear velocity would cause saltation of these coarse grains, which, as already discussed, is not compatible with the observed spatial sorting. The minimum formative winds can be estimated as  $0.7 u_{*c}$  for the hematitic fragments, or  $u_* = 2.5$  m/s ( $u_{z=1} = 49$  m/s).

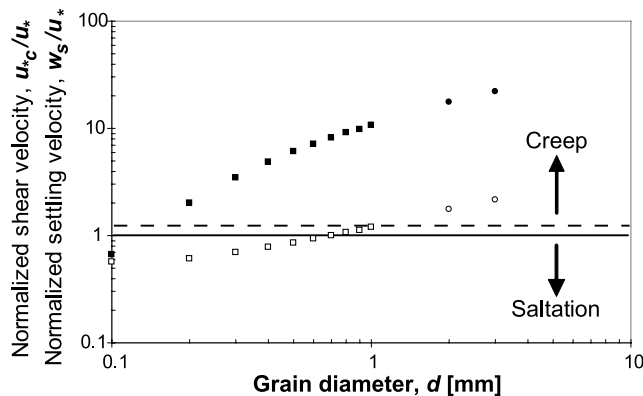


**Figure 11.** Critical shear velocity (open symbols) and settling velocity (solid symbols), normalized by measured shear velocity  $u_* = 0.41$  m/s, for representative grain sizes of gypsum (squares,  $\rho_s = 2380$  kg/m<sup>3</sup>) and rock fragments (circles,  $\rho_s = 2630$  kg/m<sup>3</sup>) observed at White Sands. Solid line shows expected transition from saltation to creep, and dotted line shows observed transition.

[39] A natural question is whether the formative wind conditions are acting today. The shear velocity required to move basaltic fines on a homogeneous bed is  $u_{*c} = 1.5$  m/s. Between ripple crests, however, these particles are shielded by spherules and fragments which cover almost 50% of the surface area. As mentioned, these larger grains extract momentum from the flow and hence increase the shear velocity required to move the finer grains in the interstices. *Gillette and Stockton* [1989] performed a series of experiments in which nonerodible glass spheres of various diameters and fractions of cover were placed over a bed of erodible sediment in a wind tunnel. Their experiments with nonerodible grains having  $d_{50}$  of 2.4 mm and 4.3 mm with spatial coverage of 45%, and eroding grains of  $d_{50} = 0.107$  mm, match very closely the geometrical properties of Meridiani ripple troughs. For these conditions, *Gillette and Stockton* [1989] found that shear velocity for initiation of motion of the fine grains increased by a factor of 2.5 in the presence of larger, nonerodible elements. *Nickling and McKenna Neuman* [1995] performed similar experiments, except that the nonerodible elements were first covered with fines; they found for their range of experiments that sediment flux decreased to near zero as a lag of nonerodible grains emerged on the surface owing to deflation. Their nonerodible elements were much larger ( $d_{50} = 18$  mm), and erodible grains were larger than those seen at Meridiani ( $d_{50} = 0.27$  mm), but experiments yielded an increase in shear velocity required to move grains by a factor of about 2, close to the value found by *Gillette and Stockton* [1989].

[40] Applying the average of the *Gillette and Stockton* [1989] and *Nickling and McKenna Neuman* [1995] results to the ripple troughs at Meridiani yields a critical shear velocity for moving the protected basaltic sand grains of  $2.25 u_{*c} = 3.4$  m/s ( $u_{z=1} = 68$  m/s). At first glance it might seem remarkable that this is the same shear velocity required to initiate motion of the hematitic fragments on the ripple crests, but this result should be expected because the same wind moving particles on ripple crests also affects the ripple troughs. This implies that the present surface at the Opportunity landing site between Eagle and Endurance craters is in an approximate state of equal threshold mobility, with bed topography and textures consistent with a single wind-forming condition. The textural composition of the surface evolved from a heterogeneous mixture of grains until a coarse armor had concentrated in the ripple troughs enough to inhibit further erosion of fines. The surface may then have ceased to evolve, or may be active only during extreme modern wind conditions. In other words, winds near  $u_* = 3.5$  m/s ( $u_{z=1} = 70$  m/s) sculpted the surface, and winds at least this strong are required to re-mobilize grains in the current bed configuration.

[41] Finally, we consider the conditions that would be required to move the hematitic spherules found in the inter-ripple zones. From (4) we find that  $u_{*c} = 5.4$  m/s ( $u_{z=1} = 108$  m/s) for a diameter of 3 mm, although this value comes from assuming a bed of uniform grains. Presently, the spherules are perched on a substrate of grains having variable size, some being more than ten times smaller, and so we expect the threshold shear velocity of spherules to be reduced [*Fenton and Abbot*, 1977; *Wiberg and Smith*, 1987]. Acknowledging that there is no definitive substrate

grain diameter owing to the heterogeneity of the soil, we choose a representative median diameter of 1 mm from our grain size distributions in Figure 7b. We find that the ratio of spherule diameter to median substrate diameter is approximately 3. According to the analysis of *Wiberg and Smith* [1987] the critical shear velocity of Meridiani spherules found in ripple troughs would be reduced by a factor of about  $\sqrt{3}$  compared to the case of a bed of uniform spherules. This estimate is very crude, but it suggests that the critical shear velocity for initiation of motion of spherules is 3.2 m/s. This value is close to the estimated threshold condition of motion for the Opportunity landing site discussed above, and it supports the notion that the plains in this area have evolved to a state of equal threshold mobility by a common wind.

### 5.3. Dust Streaks at Opportunity Landing Site

[42] High wind speeds on the surface at the Opportunity landing site today are constrained by the threshold for entrainment of dust into suspension required to reform dust streaks [*Sullivan et al.*, 2005]. Dust is so small that, once entrained, the particles go directly into suspension. The threshold shear velocity for entrainment of dust has been examined experimentally under Martian conditions by *White et al.* [1997] and *Greeley et al.* [2000]. For a smooth homogeneous surface,  $u_{*c}$  for dust is approximately 3 m/s [*White et al.*, 1997]. The presence of roughness elements changes  $u_{*c}$ ; for entrainment of dust on exposed pebble tops this value is 2 m/s [*White et al.*, 1997; *Greeley et al.*, 2000], while protected dust between pebbles can have a much larger value, up to  $u_{*c} = 4.5$  m/s. It is not known whether the mobilization of dust involved with dust streak reorientation penetrates between pebbles on the surface, or merely clears off pebble tops. We infer then that surface wind conditions at the Opportunity landing site during dust-lifting events are  $u_* \geq 2.0$  m/s ( $u_{z=1} \geq 40$  m/s).

## 6. Conclusions

[43] We have outlined a method showing how spatial grain size sorting can be used to infer transport modes, and we have estimated maximum and minimum wind speeds required to form observed ripple features on the basis of considerations of threshold of motion and settling velocity. The classic proposed mechanisms for development of terrestrial coarse-grained ripple formation have been confirmed quantitatively from observations collected at White Sands National Monument. The pattern and texture of grains seen at the Opportunity landing site, Meridiani Planum, Mars, along with ripple morphology, are used to infer that these ubiquitous features are coarse-grained ripples that formed in a manner similar to terrestrial coarse-grained ripples, by the processes described herein. Resolving grain sizes using MI images, coupled with Pancam and Navcam images for context, have allowed us to tightly constrain the wind conditions responsible for development of these ripples mantling the plains of the Opportunity landing site. The method outlined here should be applicable to any planetary surface where sufficient data are available, inasmuch as relations for settling velocity (3) and threshold of motion (4) are universal.

[44] For a bed of fairly uniform grain size, the minimum formative wind speed can be estimated using the threshold shear velocity of the median grain diameter calculated from equation (4); however, no reasonable maximum bound can be inferred. The situation is different for a heterogeneous soil because a given wind spatially sorts grains by selective transport, and hence the distribution of grain sizes on the surface can provide both a minimum and maximum estimate of wind speed. Formative conditions for coarse-grained ripples are well constrained by the simple expression  $0.7u_{*c} \leq u_* \leq u_{*c}$ , where  $u_{*c}$  is the threshold of motion for the median diameter of the coarse-grain population on ripple crests [Bagnold, 1941]. Coarse-grained ripples at the Opportunity landing site between Eagle and Endurance craters formed during conditions  $2.5 \text{ m/s} \leq u_* \leq 3.5 \text{ m/s}$ , likely closer to  $u_* = 3.5 \text{ m/s}$  ( $u_{z=1} = 70 \text{ m/s}$ ). The plains at the Opportunity landing site today have evolved to a state of equal threshold mobility such that  $u_* \geq 3.5 \text{ m/s}$  would be required to activate coarse-grained ripples and inter-ripple zones. This threshold condition requires a wind speed that is less than a factor of 2 larger than the minimum inferred during modern dust-clearing events,  $u_* = 2.0 \text{ m/s}$  ( $u_{z=1} = 40 \text{ m/s}$ ), so coarse-grained ripples may have been active relatively recently. The multiple orientations of coarse-grained ripple crests (Figure 2) implies a changing wind direction [Sullivan *et al.*, 2005], and our analysis suggests that it is possible these ripples were re-mobilized by wind as recently as the past decade.

[45] Eolian processes have long shaped the surface of Mars, and because of the dominance of wind over much of its history, eolian features may constitute a large fraction of sedimentary deposits. Wind at Meridiani Planum has sorted and concentrated hematitic concretions and their fragments, whose spectral properties from the ground [Christensen *et al.*, 2004; Soderblom *et al.*, 2004] match orbital spectra [Christensen *et al.*, 2000]. The detection of hematite was the mineralogical beacon that Opportunity was sent to explore [Christensen *et al.*, 2000; Golombek *et al.*, 2003]. In a surprising consequence of planetary history, the discovery of ancient sedimentary deposits of aqueous origin may have been facilitated by the action of recent winds.

## Appendix A

### A1. Particle and Fluid Timescales

[46] A certain amount of time is required for a grain in motion to respond to turbulent fluctuations in the fluid velocity because it has inertia. The response time or inertial time,  $t_R$ , for a grain in a given fluid can be estimated as [Snyder and Lumley, 1971]

$$t_R = \frac{w_s}{g}. \quad (\text{A1})$$

The characteristic timescale of turbulent eddies in a boundary layer flow,  $T_E$ , increases with distance from the bed as a consequence of equation (2) [e.g., Nishimura and Hunt, 2000],

$$T_E = \frac{z}{2u_*}. \quad (\text{A2})$$

For particles in which  $t_R \gg T_E$ , turbulent velocity fluctuations do not affect transport significantly and the

mean fluid shear velocity is adequate to characterize sediment transport. For the case where  $T_E \gg t_R$ , velocity fluctuations cannot be neglected. For a grain of gypsum ( $\rho_s = 2380 \text{ kg/m}^3$ ) with  $d = 0.6 \text{ mm}$ , particle response time is equal to 0.01 s, 0.31 s and 2.30 s for cases of underwater on Earth, the terrestrial atmosphere and the Martian atmosphere, respectively. The eddy timescale at an elevation of 0.10 m above the bed for the threshold-of-motion condition for each scenario is 2.27 s, 0.12 s and 0.04 s, respectively. From the simple relations (A1) and (A2) we expect that velocity fluctuations strongly affect sediment transport underwater, but are negligible for near-bed transport in the atmosphere of both Earth and (even more so) Mars. Observations underwater and in air on Earth support these results, and so it is likely a very good assumption that velocity fluctuations can be neglected when estimating initiation of motion and saltation transport on Mars.

### A2. Suspension Criterion

[47] The ratio of particle settling velocity to fluid shear velocity has been used to characterize the mode of sediment transport (e.g., saltation or suspension) for terrestrial underwater studies since Rouse [1939] [see also Bagnold, 1966; Niño *et al.*, 2003], and also for eolian studies in terrestrial [Bagnold, 1941; Chepil, 1945; Nishimura and Hunt, 2000; Shao, 2000] and Martian [Sagan and Bagnold, 1975; White, 1979; Iversen and White, 1982; Greeley and Iversen, 1985; Sullivan *et al.*, 2005] atmospheric conditions. Although there is considerable variability, well-controlled terrestrial subaqueous and eolian experiments converge on  $w_s/u_* = 1$  as a rough value for the transition to suspension. Some of this variability is because the transition to suspension is gradual and hence defining suspension is subjective. Shao [2000] suggests a value of  $w_s/u_*$  for “pure” suspension equal to 0.5 from terrestrial eolian work, which is corroborated by terrestrial subaqueous experiments [e.g., Niño *et al.*, 2003].

[48] Sullivan *et al.* [2005] suggest that  $w_s/u_*$  for suspension may be different on Mars as compared to Earth because particle response time in the thin Martian atmosphere would be larger. Although particle response time changes as a function of fluid properties (see above), the transition to suspension does not change systematically with fluid density and viscosity under terrestrial conditions. In other words, particles on Earth enter into suspension when upward directed turbulent velocity fluctuations exceed particle settling velocity, regardless of fluid density and viscosity. We expect then that  $w_s/u_* < 1$  defines the transition to suspension in the Martian atmosphere as well, in contrast to the claim of White *et al.* [1997] that suspension occurs at a much lower value,  $w_s/u_* < 0.14$ . A more detailed experimental study of suspension under Martian conditions, in which sediment flux profiles, grain size and grain trajectories are well characterized, may settle the issue of whether the particle suspension criterion is different under Martian atmospheric conditions.

[49] **Acknowledgments.** Ian Garrick-Bethell, Joel Johnson, Brandon McElroy, Anna Monders, Will Oumet, John Southard, and Kyle Straub were part of the data collection and processing team for the field campaign at White Sands. John Southard and Robert Sullivan contributed key insights regarding sediment transport, and helpful comments that improved this manuscript. MER scientists Jeffrey Johnson, Scott

McLennan, and Christian Schröder also provided helpful comments. Bill Conrod and crew of White Sands National Monument are thanked for their enthusiastic support in terms of logistics and guidance in the field. Reviews by David Baratoux, Nicholas Lancaster, and Ken Edgett improved the clarity and scope of this manuscript, and were facilitated by the balanced editing of Jeff Plescia. Our gratitude is extended to the entire MER science and engineering team for data collection and support. This work was performed for the Jet Propulsion Laboratory, California Institute of Technology, under a contract with the National Aeronautics and Space Administration.

## References

- Anderson, R. S., and K. L. Bunas (1993), Grain size segregation and stratigraphy in aeolian ripples modeled with a cellular automaton, *Nature*, *365*, 740–743.
- Anderson, R. S., and P. K. Haff (1988), Simulation of eolian saltation, *Science*, *241*, 820–823.
- Bagnold, R. A. (1941), *The Physics of Blown Sand and Desert Dunes*, Methuen, New York.
- Bagnold, R. A. (1966), An approach to the sediment transport problem for general physics, *U.S. Geol. Surv. Prof. Pap.*, 422-I.
- Chepil, W. S. (1945), Dynamics of wind erosion: I. Nature of movement of soil by wind, *Soil Sci.*, *60*, 305–320.
- Christensen, P. R., et al. (2000), Detection of crystalline hematite mineralization on Mars by the Thermal Emission Spectrometer: Evidence for near-surface water, *J. Geophys. Res.*, *105*, 9623–9642.
- Christensen, P. R., et al. (2004), Mineralogy at Meridiani Planum for the Mini-TES experiment on the Opportunity Rover, *Science*, *306*, 1733–1739.
- Cornelis, W. M., and D. Gabriels (2004), A simple model for the prediction of the deflation threshold shear velocity of dry loose particles, *Sedimentology*, *51*, 39–51.
- Ellwood, J. M., P. D. Evans, and I. G. Wilson (1975), Small scale aeolian bedforms, *J. Sediment. Petrol.*, *45*, 554–561.
- Fenton, J., and J. E. Abbot (1977), Initial movement of grains on a stream bed: The effect of relative protrusion, *Proc. R. Soc. London, Ser. A*, *352*, 523–537.
- Ferguson, R. I., and M. Church (2004), A simple universal equation for grain settling velocity, *J. Sediment. Res.*, *74*, 933–937.
- Fisher, J. S., B. L. Sill, and D. F. Clark (1983), Organic detritus particles: Initiation of motion criteria on sand and gravel beds, *Water Resour. Res.*, *19*, 1627–1631.
- Fryberger, S. G., P. Hesp, and K. Hastings (1992), Aeolian granule ripple deposits, Namibia, *Sedimentology*, *39*, 319–331.
- Gillette, D., and P. A. Goodwin (1974), Microscale transport of sand-sized soil aggregates eroded by wind, *J. Geophys. Res.*, *79*, 4080–4084.
- Gillette, D. A., and P. H. Stockton (1989), The effect of nonerodible particles on wind erosion of erodible surfaces, *J. Geophys. Res.*, *94*, 12,885–12,893.
- Golombek, M. P., et al. (2003), Selection of the Mars Exploration Rover landing sites, *J. Geophys. Res.*, *108*(E12), 8072, doi:10.1029/2003JE002074.
- Greeley, R., and J. D. Iversen (1985), *Wind as a Geological Process*, 333 pp., Cambridge Univ. Press, New York.
- Greeley, R., D. G. Blumberg, and S. H. Williams (1996), Field measurements of the flux and speed of wind-blown sand, *Sedimentology*, *43*, 41–52.
- Greeley, R., G. Wilson, R. Coquilla, B. White, and R. Haberle (2000), Windblown dust on Mars: Laboratory simulations of flux as a function of surface roughness, *Planet. Space Sci.*, *48*, 1349–1355.
- Grotzinger, J. P., et al. (2005), Stratigraphy and sedimentology of a dry to wet eolian depositional system, Burns Formation, Meridiani Planum, Mars, *Earth Planet. Sci. Lett.*, *240*, 11–72.
- Herkenhoff, K. E., et al. (2003), Athena Microscopic Imager investigation, *J. Geophys. Res.*, *108*(E12), 8065, doi:10.1029/2003JE002076.
- Iversen, J. D., and B. R. White (1982), Saltation threshold on Earth, Mars and Venus, *Sedimentology*, *29*, 111–119.
- Kellerhals, R., and D. I. Bray (1971), Sampling procedures for coarse fluvial sediments, *J. Hydraul. Eng.*, *97*, 1165–1180.
- Kellerhals, R., J. Shaw, and V. K. Arora (1975), On grain size from thin sections, *J. Geol.*, *83*, 79–96.
- Klingelhofer, G., et al. (2004), Jarosite and hematite at Meridiani Planum from Opportunity's Mössbauer Spectrometer, *Science*, *306*, 1740–1745.
- Langford, R. P. (2003), The Holocene history of the White Sands dune field and influences on eolian deflation and playa lakes, *Quat. Int.*, *104*, 31–39.
- Lee, J. A. (1987), A field experiment on the role of small scale wind gustiness in Aeolian sand transport, *Earth Surf. Processes Landforms*, *12*, 331–335.
- McKee, E. D. (1966), Structures of dunes at White Sands National Monument, *Sedimentology*, *7*, 3–69.
- McLennan, S. M., et al. (2005), Provenance and diagenesis of the evaporate-bearing Burns formation, Meridiani Planum, Mars, *Earth Planet. Sci. Lett.*, *240*, 95–121.
- Miller, M. C., and P. D. Komar (1977), The development of sediment threshold curves for unusual environments (Mars) and for inadequately studied materials (foram sands), *Sedimentology*, *24*, 709–721.
- Nalpanis, P., J. C. R. Hunt, and C. F. Barrett (1993), Saltating particles over flat beds, *J. Fluid Mech.*, *251*, 661–685.
- Namikas, S., and D. J. Sherman (1997), Predicting aeolian sand transport: Revisiting the White model, *Earth Surf. Processes Landforms*, *22*, 601–604.
- Nickling, W. G. (1983), Grain-size characteristics of sediment transported during dust storms, *J. Sediment. Petrol.*, *53*, 1011–1024.
- Nickling, W. G., and C. McKenna Neuman (1995), Development of deflation lag surfaces, *Sedimentology*, *42*, 403–414.
- Niño, Y., F. Lopez, and M. Garcia (2003), Threshold for particle entrainment into suspension, *Sedimentology*, *50*, 247–263.
- Nishimura, K., and J. C. R. Hunt (2000), Saltation and incipient suspension above a flat particle bed below a turbulent boundary layer, *J. Fluid Mech.*, *417*, 77–102.
- Pollack, J. B., R. Haberle, R. Greeley, and J. Iversen (1976), Estimates of the wind speeds required for particle motion on Mars, *Icarus*, *29*, 395–417.
- Powers, M. C. (1953), A new roundness scale for sedimentary particles, *J. Sediment. Petrol.*, *23*, 117–119.
- Rouse, H. (1939), Experiments on the mechanics of sediment transport, in *5th International Congress of Applied Mechanics*, pp. 550–554, John Wiley, Hoboken, N. J.
- Sagan, C., and R. A. Bagnold (1975), Fluid transport on Earth and aeolian transport on Mars, *Icarus*, *26*, 209–218.
- Shao, Y. (2000), *Physics and Modelling of Wind Erosion*, Springer, New York.
- Shao, Y., and H. Lu (2000), A simple expression for wind erosion threshold friction velocity, *J. Geophys. Res.*, *105*, 22,437–22,443.
- Sharp, R. P. (1963), Wind ripples, *J. Geol.*, *71*, 617–636.
- Snyder, W. H., and J. L. Lumley (1971), Some measurements of particle velocity autocorrelation functions in a turbulent flow, *J. Fluid Mech.*, *48*, 41–71.
- Soderblom, L. A., et al. (2004), Soils of Eagle Crater and Meridiani Planum at the Opportunity Rover landing site, *Science*, *306*, 1723–1726.
- Squyres, S. W., et al. (2003), Athena Mars rover science investigation, *J. Geophys. Res.*, *108*(E12), 8062, doi:10.1029/2003JE002121.
- Squyres, S. W., et al. (2004), In situ evidence for an ancient aqueous environment at Meridiani Planum, Mars, *Science*, *306*, 1709–1714.
- Sullivan, R., et al. (2005), Aeolian processes at the Mars Exploration Rover Meridiani Planum landing site, *Nature*, *436*, 58–61.
- Walker, J. D., and J. B. Southard (1984), A sticky-surface trap for sampling eolian saltation load, *J. Sediment. Petrol.*, *54*, 652–654.
- White, B. R. (1979), Soil transport by wind on Mars, *J. Geophys. Res.*, *84*, 4643–4651.
- White, B. R., B. M. Lacchia, R. Greeley, and R. N. Leach (1997), Aeolian behavior of dust in a simulated Martian environment, *J. Geophys. Res.*, *102*, 25,629–25,640.
- Wiberg, P. L., and J. D. Smith (1987), Calculations of the critical shear stress for motion of uniform and heterogeneous sediments, *Water Resour. Res.*, *23*, 1471–1480.
- Wolman, M. G. (1954), A method for sampling coarse river bed material, *Eos Trans. AGU*, *35*, 951–956.

D. A. Fike, D. J. Jerolmack, D. Mohrig, and W. A. Watters, Department of Earth, Atmospheric and Planetary Sciences, Massachusetts Institute of Technology, 77 Massachusetts Avenue, Cambridge, MA 02139, USA. (dfike@mit.edu; douglasj@mit.edu; mohrig@mit.edu; watters@mit.edu)

J. P. Grotzinger, Geological and Planetary Sciences, California Institute of Technology, M/C 170-25, 1200 East California Boulevard, Pasadena, CA 91125, USA. (grotz@gps.caltech.edu)